

# Developing a deep learning forecasting system for short-term and high-resolution prediction of sea ice concentration

Are Frode Kvanum<sup>1,2</sup>, Cyril Palerme<sup>1</sup>, Malte Müller<sup>1,2</sup>, Jean Rabault<sup>3</sup>, and Nick Hughes<sup>4</sup>

<sup>1</sup>Development Centre for Weather Forecasting, Norwegian Meteorological Institute, Oslo, Norway

<sup>2</sup>Department of Geosciences, University of Oslo, Oslo, Norway

<sup>3</sup>IT Department, Norwegian Meteorological Institute, Oslo, Norway

<sup>4</sup>Ice Service, Norwegian Meteorological Institute, Tromsø, Norway

**Correspondence:** Are Frode Kvanum (arefk@met.no)

**Abstract.** There has been a steady increase of marine activity throughout the Arctic Ocean during the last decades, and maritime end users are requesting skillful high-resolution sea ice forecasts to ensure operational safety. Different studies have demonstrated the effectiveness of utilizing computationally lightweight deep learning models to predict sea ice properties in the Arctic. In this study, we utilize operational atmospheric forecasts as well as ice charts and sea ice concentration passive microwave observations as predictors to train a deep learning model with future ice charts as ground truth. The developed deep learning forecasting system predicts regional ice charts covering parts of the East Greenland and Barents seas at one kilometer resolution for 1 to 3-day lead time. We validate the deep learning system performance by evaluating the position of forecasted sea ice concentration contours at different concentration thresholds. It is shown that the deep learning forecasting system achieves a lower error for several sea ice concentration contours when compared against baseline-forecasts (persistence-forecasts, sea ice free-drift and a linear trend), as well as two state-of-the-art dynamical sea ice forecasting systems (neXtSIM and Barents-2.5) for all considered lead times and seasons.

## 1 Introduction

Arctic sea ice thickness and extent have decreased since the first satellite observations were obtained (Kwok, 2018; Serreze and Meier, 2019) as a response to climate change (Notz and Marotzke, 2012) which is amplified in the Arctic region (Serreze and Barry, 2011). Summer months are experiencing the greatest loss of sea ice extent (Comiso et al., 2017), with models from the Coupled Model Intercomparison Project 6 (CMIP6) projecting the first virtually ice-free (< 1 million square km) Arctic summer before 2050 (Notz and Community, 2020). As a consequence of the sea ice retreat during the summer months, there has been an increase in maritime activity in the Arctic (Eguíluz et al., 2016; Gunnarsson, 2021) resulting in a consistent increase in the number of ships present in the Arctic. The period during which many vessels operate has also extended beyond the summer months, increasing mariners exposure to hazardous sea ice conditions (Müller et al., 2023). The influx of operators to the Arctic region has increased the demand for accurate short-range sea ice forecasts (Stocker et al., 2020), and that end-users needs are taken into account during the validation of these forecasts (Melsom et al., 2019; Wagner et al., 2020).

Although dynamical sea-ice forecasting systems have been producing operational forecasts at different resolutions and lead times e.g. (Sakov et al., 2012; Metzger et al., 2014; Williams et al., 2021; Röhrs et al., 2023), feedback from maritime operators suggests that current sea ice forecasts lack sufficient and relevant verification (Veland et al., 2021). Consequently, maritime operators tend to rather rely on their own experience (Blair et al., 2022) despite the improved situational awareness provided by sea ice forecasts for tactical navigation (Rainville et al., 2020). Moreover, dynamical forecasts are computationally expensive, especially when targeting high spatial resolutions. In recent years, statistical forecasting approaches have emerged where deep neural networks have been trained on past sea ice information as well as the state of the atmosphere in order to predict the future state of sea ice concentration (SIC) (e.g. Fritzner et al., 2020; Liu et al., 2021b; Andersson et al., 2021; Liu et al., 2021a; Ren et al., 2022; Grigoryev et al., 2022). These machine learning approaches require little memory and computational resources to produce a forecast, once they are trained.

Previous studies (Liu et al., 2021b; Andersson et al., 2021; Liu et al., 2021a; Ren et al., 2022) train deep learning models on reanalysis datasets such as ERA5 (0.25° resolution) (Hersbach et al., 2020) or use SIC derived from coarse resolution (25 km resolution) satellite climate data records (such as the products from Cavalieri et al. (1996) and Lavergne et al. (2019)). Andersson et al. (2021) proposed IceNet, a pan-Arctic U-Net classifying SIC into separate classes defined by sea ice concentration thresholds. Andersson et al. (2021) demonstrated that IceNet consistently improved upon the seasonal numerical forecasting system SEAS5 (Johnson et al., 2019) for lead times of 2 months and longer. Similarly, Liu et al. (2021b) showed that a convolutional long short-term memory network covering the Barents Sea with a 6 week lead time directly predicting SIC was more skillful than persistence for all considered weekly lead times. However, due to the aforementioned models using climatological-scale data as predictors and ground truth, their application to maritime users as short term operational forecasts are limited (Wagner et al., 2020).

Grigoryev et al. (2022) presented a multi-regional U-Net forecasting system predicting SIC for lead times up to 10 days where the real-time availability of SIC satellite retrievals and numerical weather forecasts were considered. The deep learning forecasts of Grigoryev et al. (2022) considerably outperformed persistence and linear trend baseline forecasts in the considered regions of the Barents, Labrador, and Laptev Seas. Fritzner et al. (2020) demonstrated the possibility of utilizing a fully convolutional network to forecast ice charts for the region around Svalbard and the Barents Sea, however the forecasts had a coarse spatial resolution due to limited computational resources. High resolution sea ice forecasts are important for this region as it is the focus of many commercial operators from different maritime sectors such as shipping, fishing and tourism (Stocker et al., 2020; Müller et al., 2023).

In this paper we present the development of a regional deep learning forecasting system targeting 1 km spatial resolution and 1 – 3 day lead time covering the area around Svalbard and the Barents Sea. The choice of predictors and target data is made with operational concerns, and the quality of the forecasts is assessed against relevant baseline forecasts and dynamical sea ice forecasting systems in a manner relevant for end-users (Melsom et al., 2019; Wagner et al., 2020). The impact from the different predictors is also assessed. Section 2 describes the datasets used for this study, followed by Section 3 presenting the neural network implementation and verification setup. Section 4 presents the results, with Section 5 providing the discussions and conclusions.

2 Data

To develop the deep learning forecasting system, several observation and physical model forecasting system datasets have been chosen as predictors, targets and for validation. When selecting appropriate datasets, their spatial resolution as well as release frequency has been considered in order to develop an operational product. Table 1 presents the different products we have used, as well as the role they play in our forecasting system which will be further described in the following sections. The region of interest is depicted in Fig. 1 and is constructed as an intersection between the regional domains of the gridded ice chart data produced by the Norwegian Ice Service (<https://cryo.met.no/en/latest-ice-charts>) and the regional numerical weather prediction system AROME Arctic (Müller et al., 2017). The deep learning model has been developed using the U-Net architecture (Ronneberger et al., 2015), which requires the spatial dimensions of the input fields to be repeatedly divisible by a given factor a number of times. For simplicity, the model domain was set to be a one kilometer spatial resolution square grid containing  $1792 \times 1792$  equidistant grid-cells, which is four times divisible by 4. This domain was achieved by removing lower latitudes from the original AROME Arctic domain, affecting the southern Norwegian, Barents and Kara seas.

**Table 1.** Products used, their application as well as temporal regime. Observational products and physical forecasting models are separated by descriptive italic text. Time regime refers to which time period the dataset covers with respect to the initialization date of the deep learning model.

| Product             | Variables      | Training           | Validation | Time regime      |
|---------------------|----------------|--------------------|------------|------------------|
| <i>Observations</i> |                |                    |            |                  |
| Ice charts          | SIC            | Predictor / Target | Yes        | Present / Future |
| OSI SAF SSMIS       | SIC trend      | Predictor          | Yes        | Past             |
| AMSR2 (ASI)         | SIC            | No                 | Yes        | Future           |
| <i>Models</i>       |                |                    |            |                  |
| AROME Arctic        | T2M, X,Y-Winds | Predictor          | No         | Future           |
| NeXtSIM             | SIC            | No                 | Yes        | Future           |
| Barents-2.5         | SIC            | No                 | Yes        | Future           |

2.1 Sea-ice concentration observations

The ice charts are manually drawn to deliver a SIC product which is distributed every workday at 15:00 UTC by the Ice Service of the Norwegian Meteorological Institute (<https://www.cryo.met.no/en/latest-ice-charts>). The ice analyst who draws the ice chart assesses and merges available synthetic aperture radar (SAR) scenes with visible- and infrared imager observations. These data sources are supplemented by coarse resolution passive microwave observations to achieve a consistent spatial coverage. Incoming observations are interpreted by the ice analyst as they become available. For our model domain (Fig. 1) Sentinel-1

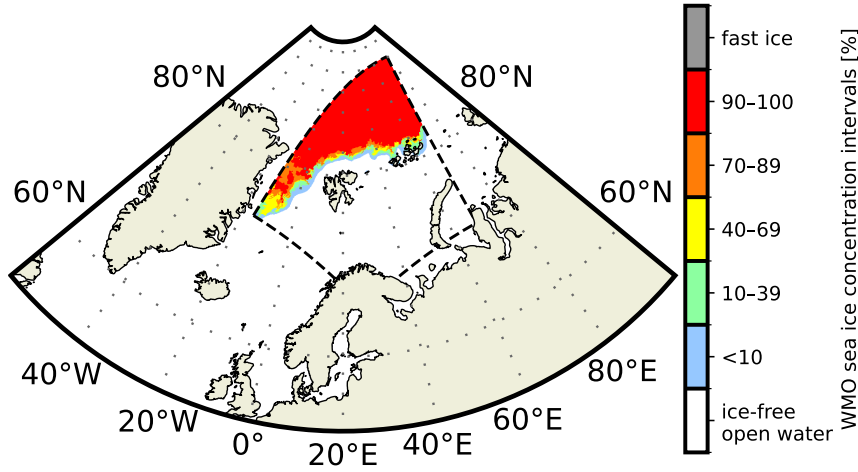


**Figure 1.** The model domain (dashed-contour) together with the SIC retrieved from a ice chart (15 sep 2022). The SIC intervals and color code follows the WMO Ice Chart Colour Standard and Sea Ice Nomenclature.

SAR swaths are available between midnight and 08:00 UTC starting from Novaya-Zemlya. Following a consideration of input data availability and ice analyst judgement, we assume the ice charts to reflect the sea ice state at 12:00 UTC.

We use gridded SIC from the ice charts as both a predictor representing initial sea ice conditions and a target at 1 – 3 day lead time since the product captures daily (weekdays from Monday to Friday) observed SIC at a high ( $\leq 1\text{km}$ ) spatial resolution.

80 The ice charts are a categorical product, with SIC following the World Meteorological Organization (WMO) total concentration intervals (see colorbar of Fig. 1). For this study, the ice charts have been gridded from vector polygons onto the model domain with a 1 km spatial resolution using nearest neighbor interpolation. Moreover, we have filtered out Baltic sea ice as the task of the deep learning system in this study is to predict sea ice in the Greenland and Barents seas.

In addition to the ice charts, SIC observations from the Ocean and Sea Ice Satellite Application Facility (OSI SAF) Special  
85 Sensor Microwave Imager/Sounder (SSMIS) (OSI-401) and AMSR2 observations processed with the ASI algorithm from the University of Bremen (Spren et al., 2008) are utilized. OSI SAF SSMIS is supplied on a 10 km spatial resolution, and will be used to compute a linear sea-ice concentration trend which will serve as both a predictor and as a baseline-forecast for validation. Motivated by the lack of temporal awareness of the U-Net architecture (Ronneberger et al., 2015), computing a linear trend from past sea-ice concentration fields will encode multiple previous time-steps into a single two dimensional field.  
90 Moreover, computing the linear trend from a different product than the ice charts will supply the model with correlated but not

overlapping information. It is also noted that the ice charts are not produced every day, hence it would not be possible to use the product to compute a local trend.

AMSR2 observations are used for validation of the deep learning forecasting system only. The AMSR2 data utilized for this work is the ASI sea-ice concentration product from the University of Bremen (Spreen et al., 2008). The dataset is provided on a 6.25 km grid. AMSR2 observations can be considered as an independent product from the ice charts which are primarily derived from SAR observations, and are not used to train the deep learning model. Hence, the AMSR2 data are used as an external product for validation of forecast performance, providing an estimation of the deep learning model's ability to provide consistent forecasts beyond using the ice charts as validation.

## 2.2 Physical forecasting systems

In addition to training the deep learning model on current and previous sea-ice concentration data, we also include atmospheric predictors as it has been demonstrated that the inclusion of the present- and future state of the atmosphere can improve the sea-ice predictions from deep learning (Grigoryev et al., 2022; Palerme et al., 2024). For this study, forecasts of 2-meter temperature and the 10-meter wind components adjusted to align with the x,y dimensions of the model grid (x,y-wind) were taken from the AROME Arctic regional numerical weather prediction system developed for operations at the Norwegian Meteorological Institute (Müller et al., 2017). Although not a forecast field, the land-sea mask used in AROME Arctic is also extracted as a predictor. We use AROME Arctic forecasts as predictors for this study due to its high spatial resolution and regional coverage of the European Arctic. AROME Arctic runs up to 66 hours lead time, is supplied on a 2.5 km resolution grid with 66 vertical levels, and a new forecast is initiated every six hours. Near surface winds influence the sea ice drift following a non-linear relationship between wind speed, sea-ice drift speed, sea-ice concentration and sea-ice thickness (Yu et al., 2020). Moreover, near surface temperatures affects the sea-ice through melting or growth. AROME Arctic has been in operation and continuous development since October 2015, routinely receiving updates which introduce permanent bias changes for predicted variables. Due to a major change to the representation of snow over sea-ice in 2018, a warm bias in near-surface temperatures above sea-ice was significantly reduced in the model (Batrak and Müller, 2019). Thus we start our training dataset at 2019 to avoid supplying our deep learning model with samples containing different temperature biases, especially close to the marginal ice zone (MIZ) where the greatest model response to predictors occurs.

Moreover, the two short-range sea-ice forecasting systems neXtSIM-F (Williams et al., 2021) and Barents-2.5 (Röhrs et al., 2023) are used to validate the deep learning forecasts against high-resolution physical forecasting systems. neXtSIM-F is based on the neXtSIM sea-ice model which is a dynamical/thermodynamical sea-ice model using a brittle rheology (Rampal et al., 2016). The version of neXtSIM used for this work uses the Brittle Bingham Maxwell rheology (Ólason et al., 2022). NeXtSIM receives oceanic forcing from TOPAZ4 (Sakov et al., 2012) and atmospheric forcing from ECMWF IFS (Owens and Hewson, 2018). The forecasts are supplied on a pan-Arctic grid at 3 km resolution. Barents-2.5 is a regional ocean and sea-ice ensemble forecasting system developed at the Norwegian Meteorological Institute (Röhrs et al., 2023), and is produced on a 2.5 km spatial resolution and runs up to 66 hours lead time on the same grid as AROME Arctic. The sea-ice model used in Barents-2.5 is CICE (Hunke et al., 2015). At prediction time, six members are initiated, with one member receiving atmospheric forcing

125 from AROME Arctic and the rest by atmospheric forecasts from ECMWF, however for this study only the member forced by AROME Arctic has been considered. Finally, due to recent developments of the model, only forecasts starting from June 2022 have been considered from Barents-2.5.

### 3 Methodology

#### 3.1 Dataset preprocessing and selection

130 We perform preliminary computations in order to ensure that the data from different sources are on a common grid. The data preprocessing is performed in two stages. Firstly data not matching the AROME Arctic projection are reprojected. Secondly, for data available at a coarser resolution, nearest neighbor interpolation is performed in order to resample the data onto a 1 km grid. The U-Net architecture requires all predictors to have valid values in all grid cells, however both the input and target ice charts and SIC trend do not consistently represent SIC for land covered grid cells due to their intended unavailability. In  
135 order to avoid sharp gradients between sea-ice covered seas and land covered areas in the ice charts and SIC trend, we apply a nearest neighbor interpolation of the local sea-ice conditions to fill in the missing sea-ice concentration over land grid points following Wang et al. (2017).

Since all the datasets we use for training come from operational products, we have to take into account production- and publishing time as well as forecast length when selecting predictors. A graphical summary of the operational schedule for  
140 predictor selection is shown in Fig 2. The ice charts are valid at 12:00 UTC, which will be regarded as the initialization time for the deep learning forecasts. The OSI SAF linear trend is computed from the five previous days, until the day before deep learning forecast initialization. We want AROME Arctic forecasts to provide the future state of the atmosphere to the deep learning system, which we set to lead times beyond deep learning initialization time. Hence it follows that the atmospheric forecast should cover the time between input and target ice chart valid time.

145 We choose to use AROME Arctic forecasts initiated at 18:00 UTC on the same day as ice chart publication. Furthermore, we set AROME Arctic forecast reference time to be 12:00 UTC on prediction-day regardless of model lead time of 1, 2 or 3-day. This way, we ensure that atmospheric forecasts cover the time period in between ice chart publication and intended target lead time. Moreover, AROME Arctic initiated at 18:00 UTC reaches 12:00 UTC for a 3-day target lead time after 66 hours (the longest lead time available from AROME Arctic forecasts), which motivates the choice of having 12:00 UTC as reference  
150 time regardless of target lead time. In addition, AROME Arctic has a production time of about 2.5 hours, which ensures that forecasts initiated at 18:00 UTC are available before midnight, allowing us to publish deep learning forecasts on the same day as the input ice chart is published.

When selecting atmospheric forecasts initiated at 18:00 UTC, six hours of future atmospheric development occurring after ice chart valid time (12:00 UTC) is not included in the atmospheric predictors. Although AROME Arctic is also initiated at  
155 12:00 UTC, the forecast initiated at 18:00 is more up to date, and as such is assumed to be more reliable especially at longer lead times. Moreover, the impact of appending six hours of AROME Arctic initialized at 12:00 UTC to the training data has been tested and shown to have an insignificant impact to model performance (see the Supplement). Finally, the ice charts do not

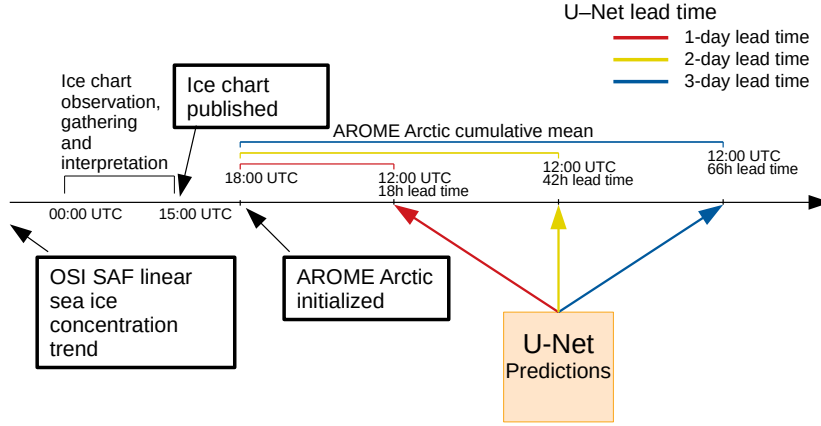


**Figure 2.** Overview diagram describing predictor publication scheduling, selection and preprocessing. Description of when the different predictors are published in relation to a published ice chart when constructing a single sample for a given date. The ice charts are published at 15:00 UTC, followed by AROME Arctic initialized 18:00 UTC (available ~ 20:30 UTC). The different colors refer to deep learning forecast lead time.

represent the sea ice state at any given lead time, rather they are a mean representation of previous observations accumulated over time ending at publication time. Hence we assume regardless of AROME Arctic initialization time that there will be some irreducible timing difference between the sea ice state from the ice charts and the initial atmospheric state from AROME Arctic, which also varies spatially.

Instead of loading multiple high-resolution AROME Arctic fields during training, we preprocess atmospheric variables during dataset creation to reduce the amount of memory needed to load predictors during training. We reduce the atmospheric forecast fields between start-date and 12:00 UTC at target date along the temporal dimension into a mean field. As well as reducing the memory footprint of each predictor, reducing the time steps into a mean-value field also accumulates the temporal changes of each atmospheric variable into a single predictor. Aggregating statistics at an increasing temporal range causes atmospheric predictors to be dependent on target lead time. Hence deep learning models are trained independently for each target lead time.

The main dataset we use covers the period between 2019 and 2022. We further split the data such that 2019 – 2020 is used for training, 2021 is used for validation and 2022 is the test dataset. Table 2 provides an overview of the number of available samples for each year given each model target lead time. Moreover, the predictors are normalized according to the min-max normalization equation. This normalization scheme ensures that the different predictors are in the same numerical range  $[0, 1]$  and that predictors can be drawn from non-normal distributions such as the ice charts. Finally, with this scheme we can combine categorical predictors from the ice charts with continuous predictors from AROME Arctic.

**Table 2.** Subset affiliation and number of samples for each year over the different target lead times.

| year | subset     | 1-day lead time | 2-day lead time | 3-day lead time |
|------|------------|-----------------|-----------------|-----------------|
| 2022 | test       | 196             | 147             | 142             |
| 2021 | validation | 198             | 147             | 142             |
| 2020 | train      | 198             | 146             | 142             |
| 2019 | train      | 192             | 143             | 144             |

Due to the routine lack of ice charts during weekends, there is a limited number of dates that can be used for training and verification, and the sample size depends on lead time as shown in Table 2. Comparing the similarly sized 2 and 3-day lead time datasets against the number of samples at 1-day lead time reveals an approximate 25% reduction in the number of available dates that is consistent for all considered years. This has implications when the ice charts are used to evaluate deep learning forecast performance because verification scores for models targeting different lead times get computed from different sets of dates.

### 3.2 Cumulative contours

Norwegian ice charts represent SIC in unevenly sized concentration categories, hence we treat the prediction of an ice chart as a classification task. For automated ice charting, Kucik and Stockholm (2023) have reported that the Categorical Cross-Entropy loss function achieves the highest rate of true positive predictions. However, ice charts are heavily imbalanced fields mostly populated with *ice-free open water* (0%) and *very close drift ice* ( $\geq 90\%$ ), and neural networks trained with Categorical Cross-Entropy tend to prioritize predicting the most frequently occurring classes while making fewer true positive predictions for intermediate SIC categories (Kucik and Stockholm, 2023).

Motivated by the skewed SIC distribution between the categories which constitutes the MIZ, we reformulate the target SIC such that each category is defined cumulatively and predicted independently using the six SIC thresholds 0, 10, 40, 70, 90% and *fast ice* (as shown in Fig. 1). Cumulative contours are a novel reformulation of the SIC prediction task which aims to preserve the ice chart category distribution. Our proposed target reformulation redefines a categorical ice chart into separate binary fields each containing SIC equal to or greater than a given SIC threshold. With cumulative contours, we provide our deep learning model binary targets which resolve each SIC category with a greater spatial balance than the multi-class ice chart.

The cumulative contours are defined as follows. We define  $N$  thresholds  $k_n \in [0, 1]$  which are ordered from lowest to highest with  $N$  being the number of contours we want to threshold. Each threshold  $k_n$  represents a SIC value and is used to classify an ice chart  $S$  into a binary field  $C^n$ , which we denote a cumulative contour. Each element in  $C^n$  is defined with the following



equation, where  $i, j$  denotes spatial indexes

$$c_{i,j}^n = \begin{cases} 1 & \text{if } s_{i,j} \geq k_n \\ 0 & \text{if } s_{i,j} < k_n \end{cases} \quad (1)$$

200 The target reformulation into cumulative contours reduces the classification task into multiple independent binary predictions. Each cumulative contour includes SIC above a set threshold, ensuring that categories in the MIZ are not underestimated due to underrepresentation in the target dataset. We assume each cumulative contour to be ordered such that  $C^{n+1} \subset C^n$ , however the deep learning model predicts each cumulative contour independently and can deviate from this assumption. We ensure that the predicted cumulative contours at each grid cell achieve the desired ordering by setting all cumulative contours  
205 proceeding a not predicted contour to 0 regardless of the probability assigned by the deep learning model.

Finally, the forecasted SIC field  $\hat{S}$  is defined as the element-wise sum over all remaining predicted cumulative contours:

$$\hat{S}_{i,j} = \sum_{\text{for all } n} \hat{c}_{i,j}^n. \quad (2)$$

where each element  $\hat{S}_{i,j} \in [0, \dots, N]$  is a categorical representation of ice chart SIC in increasing order. For this work, we have defined six thresholds  $k$  following the six WMO ice concentration intervals used in the ice charts. Thus  $\hat{S}_{i,j} = 0$  is *ice-free*  
210 *open water* and  $\hat{S}_{i,j} = 6$  is *fast ice*.

### 3.3 Model implementation

The U-Net architecture was initially developed for computer vision tasks, specifically semantic image segmentation, and expands the fully convolutional architecture introduced in Long et al. (2015) by constructing a symmetric encoder-decoder structure and adding skip-connections between the contracting and expansive paths (Ronneberger et al., 2015). Our U-Net  
215 implementation follows the original encoder-decoder structure, however the output layer has been modified in order to reflect the reformulated target SIC cumulative contours. The encoder is initiated with 64 feature maps, and at each stage we double the number of feature maps. We established through testing that the model performed optimally with a bottleneck of 256 feature maps, resulting in a three stage encoder. The spatial resolution is lowered by a factor of four at each stage due to average pooling with a  $4 \times 4$  filter. Note that the average pooling layer used here deviates from the max-pooling layer used in the original  
220 U-Net architecture, as we found through tests that average pooling tended to increase model performance similar to the findings from Palerm et al. (2024). We further note that in the original U-Net architecture the spatial resolution of the feature maps are only lowered by a factor of 2 between each stage, however our implementation reaches the bottleneck resolution faster which further reduces the size of the models.

As a consequence of reformulating the target variable into six cumulative contours following the ice chart SIC classes, the  
225 model contains six output layers which are all located at the end of the same decoder. Each cumulative contour is predicted independently from a shared signal, and a forecasted ice chart is constructed from Eq. 2. The pixelwise binary cross-entropy loss function is computed individually for all output layer contours, and the resulting loss of the model is the sum over the

individually computed losses. We initiate the model weights using HE-initialization (He et al., 2015) since the ReLU activation function (Nair and Hinton, 2010) is used for all layers.

230 All models have been trained on a NVIDIA A100 80GB GPU using mixed precision training, which restricted the maximum batch size to four samples to fit in the GPU RAM. Consequently, we replace all batch-normalization layers in the encoder and decoder with group-normalization layers to mitigate the negative effects of using batch-normalization with small batch sizes (Wu and He, 2018). During training, we use the ADAM optimizer (Kingma and Ba, 2014) with an initial learning rate of 0.001 which we reduce by a factor of 2 every 10 epochs. After training is completed (25 epochs), the model which achieves  
235 the lowest loss on the entire validation set is selected. We chose to train for 25 epochs as the validation loss rarely improved beyond that point. The flow of data in relation to the developed model is summarized in Fig. 3. For further details regarding the implementation, we refer to the GitHub repository (see code availability section).

### 3.4 Verification metrics

We chose to focus on sea ice edge based skill metrics when validating the performance of the deep learning forecasts as  
240 such metrics are appropriate when the SIC is discretized as categorical contours. These metrics are also relevant for end users (Melsom et al., 2019; Fritzner et al., 2020; Wagner et al., 2020). Specifically, we derive the length of the sea ice edge following the method introduced in Melsom et al. (2019), and assess forecast skill using the Integrated Ice Edge Error (IIEE) (Goessling et al., 2016) normalized with the ice edge (or threshold SIC contour) length derived from the target SIC field (nIIEE). The nIIEE is chosen since it is not particularly affected by isolated ice patches (Palerme et al., 2019). Moreover, the  
245 nIIEE when normalized according to a SIC contour length, is independent to the sea ice seasonality (Goessling et al., 2016; Palerme et al., 2019; Zampieri et al., 2019), which allows for a comparison of forecast-skill across seasons. Finally, the nIIEE can be interpreted as the SIC contour displacement error between two products, which is easy to interpret and relevant to end-users (Melsom et al., 2019). To the knowledge of the authors, the nIIEE has only been assessed using coarse resolution sea-ice concentration fields. However, we compared the nIIEE computed from ice charts at 1 km spatial resolution and 10 km  
250 resolution between 2019 and 2022 and found the Pearson correlation to be 0.98, which ensures the validity of applying the nIIEE also for high-resolution SIC. For further details, see the appendix.

### 3.5 Baseline-forecasts

We compare the deep learning forecasts against three baseline-forecasts, persistence of the observations, linear trend of sea-ice concentration from OSI SAF SSMIS and a purely wind-derived sea ice motion estimation based on free-drift. The baseline-  
255 forecasts serve as a lower threshold which the deep learning system must outperform in terms of nIIEE in order to be considered skillful. A persistence forecast involves keeping the initial state of the system constant in time. The baseline-forecast based on the linear trend is created by computing a pixelwise linear trend from the previous 5 days which is used to advance the system forward in time. For clarity, the computed values are bounded to match the valid value range  $[0, 100]$ . The use of a linear SIC trend as a baseline forecast has previously been assessed in Grigoryev et al. (2022), where the authors reported that the linear  
260 trend consistently achieved a higher Mean Absolute Error than persistence.

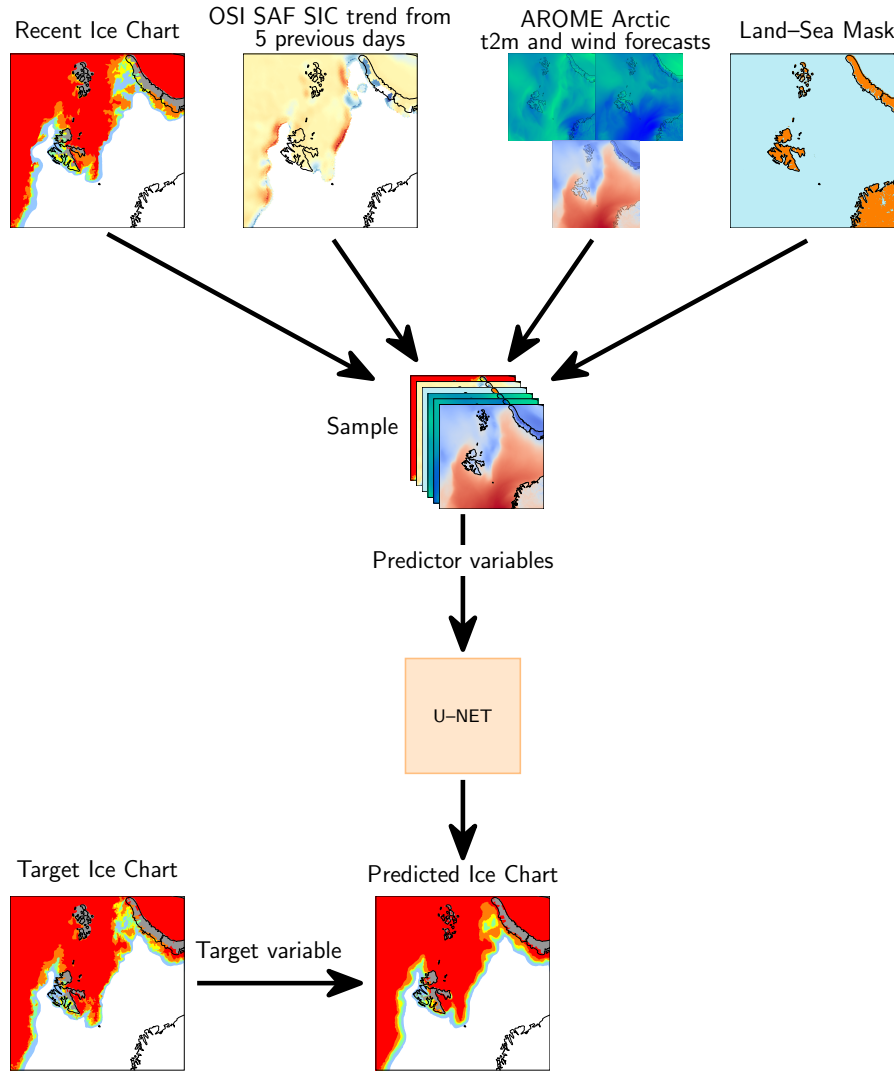


**Figure 3.** Overview of the input and output to the deep learning forecasting system. The predictors are constructed from individually preprocessed sources, and provided to the network together with an associated target ice chart.

The wind-driven free-drift baseline-forecast is implemented following the description in Zhang et al. (2024). Hence sea ice motion is estimated to be 2% of the surface wind speed 20 degrees to the right (clockwise) of the surface wind direction. Since the free-drift forecast individually advects sea ice parcels based on limited area wind-forcing, the free-drift forecast is not guaranteed to be spatially consistent as some grid cells might not be covered by sea ice after advection while they are clearly in the sea ice pack. Thus we perform nearest neighbor interpolation after advecting the ice to ensure that the free-drift forecasts are spatially consistent. In order to be consistent with the deep learning models, input SIC is advected with the same AROME Arctic mean surface wind fields also supplied as predictors to the deep learning model.

### 3.6 Model intercomparison setup

The goal of the model intercomparison is to assess the predictive skill of the deep learning forecasts against the described baseline-forecasts and physical forecasting system. In order to compare the different sea ice forecasts, all products were projected and interpolated onto the grid of the coarsest resolution product, which is neXtSIM (3 km) or AMSR2 (6.25 km) depending on which SIC product is used for evaluation. The baseline-forecasts have a daily output frequency, which is similar to the deep learning system, hence the comparison involves identifying the forecast with similar start- and target date. However, both Barents-2.5 and neXtSIM forecasts have an hourly frequency. When comparing the deep learning forecasts against both physical models, we use the physical forecasts initiated at 00:00 UTC the day following deep learning initialization. Furthermore, physical models are averaged between 00:00 UTC and 12:00 UTC on the target date of the deep learning forecast due to the ice chart production process. This setup is assumed to moderate spatial variability induced by the lack of a temporal mean.

## 4 Results

### 4.1 Training performance and data considerations

Training the deep learning system for 25 epochs takes approximately 3h30min on the A100 GPU, whereas performing a single prediction takes 6 seconds on a workstation CPU (AMD EPYC 7282 16-Core) and 30 seconds on a laptop CPU (Intel (R) Core (TM) i7-8565U 8-Core). Comparatively, a single member of Barents completes a 24-hour forecast in  $\approx 12$ min, resulting in a 99% speed up when running on comparable hardware. The optimal U-Net width of 256 channels in the bottleneck was determined by performing a grid search on the validation dataset across learning-rate (0.0001 - 0.01) and U-Net bottleneck width (256 - 1024) (see Figure S2 in the supplement). To achieve consistent architectures between the developed models, we considered only variations of the 2-day target lead time model for the grid search and reused the results for models targeting all lead times. The final model contains 2.4 million trainable parameters with 1.15 million of these being located in the encoder and 1.25 million in the decoder. We compared model implementations without cumulative contours (single output, multi-class segmentation with categorical cross-entropy loss) against deep learning models reformulated with cumulative contours, and we got a better preservation of intermediate contours with the model predicting cumulative contours, especially at longer lead times (see the Supplement). Fig. 4 presents a forecast from a deep learning model with cumulative contours targeting 2-day lead time, and shows that intermediate SIC categories have been resolved in the forecast. For the example presented in Fig. 4, the deep learning forecast achieved an nIIIE of 7.5 km while persistence achieved an nIIIE of 13.4 km. We observe in Fig. 4 that the deep learning forecast is able to reproduce the SIC increase in the Barents Sea, as well as the reduction of a polynya area north-east of Svalbard. An apparent difference between the deep learning forecast and the ice charts is that the different contours include less structural details in the deep learning forecasts, which results in a smoother appearance.

Fig. 5 compares the ability of the deep learning system to resolve sea ice categories against ice charts and AMSR2 observations. In general, the deep learning system accurately resolves the concentration category distribution in accordance with the ice charts regardless of lead time, with all categories being less than 1% different from the ice chart distribution when

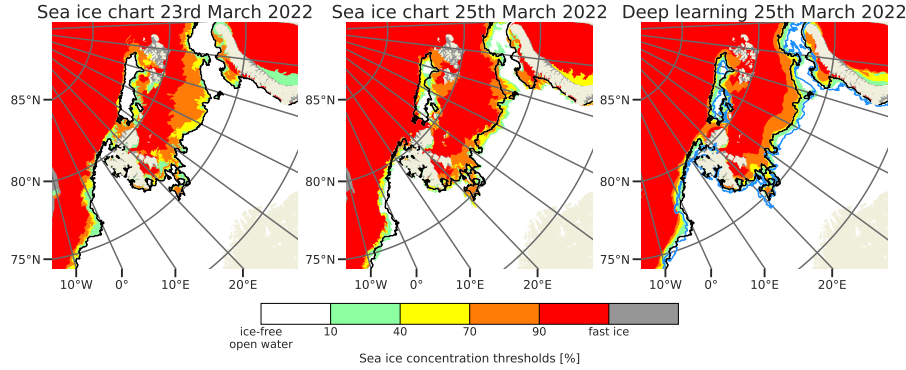


**Figure 4.** Ice charts for the 23rd (a) and 25th (b) of March 2022, with a deep learning prediction for 25th of March 2022 initialized 23rd of March 2022 in (c). The black line is the sea ice edge for the ice chart in (a) and the blue line is the sea ice edge for the ice chart in (b), both plotted for a 10% concentration threshold. The < 10% SIC category is not shown.

300 considering the yearly average. When comparing against the AMSR2 observations, it is important to note the differences in the occurrence frequency of the 100% SIC category. The ice charts consider fast-ice as a separate category representing land-fast ice, which is a distinction not made by the ASI retrieval algorithm. Although for consistency, 100% SIC from AMSR2 has been considered as *Fast ice* for this study. However the normalized integrated ice edge error only consider the lower boundary of any concentration category and as such this choice does not affect the results from the nIIEE skill score. This choice is reflected in

305 Fig. 5 where the resolved fraction of *Very close drift ice* is 20% in AMSR2 compared to 31% in the ice charts. Comparatively, the fraction of resolved *Fast ice* in AMSR2 is 8% whereas for the ice charts this category constitutes < 1% of the area.

Another difference between AMSR2 observations and the ice charts presented in Fig. 5 is how *ice-free open water* and *open water* are resolved. On a yearly average, *ice-free open water* constitutes about 62% of the AMSR2 pixels, and 55% for the ice charts. Furthermore, *open water* is more represented in the ice charts constituting about 5% of the pixels, while for the

310 AMSR2 observations this category covers only 1%. This is because the ice charts consider SAR and optical satellite retrievals with higher sensitivity to low ice concentrations to resolve *Open water*, compared to passive microwave sensors which have a low sensitivity to SIC below 15%.

## 4.2 Forecast performance and model intercomparison

We initially compare the deep learning forecasts against the baseline and dynamical forecasts in 2022 across all target lead

315 times where we consider the yearly mean of the nIIEE for different sea ice edge contours defined by (10, 40, 70 and 90%) concentration thresholds in Fig 6. For all considered lead times and concentration thresholds, the deep learning forecasts

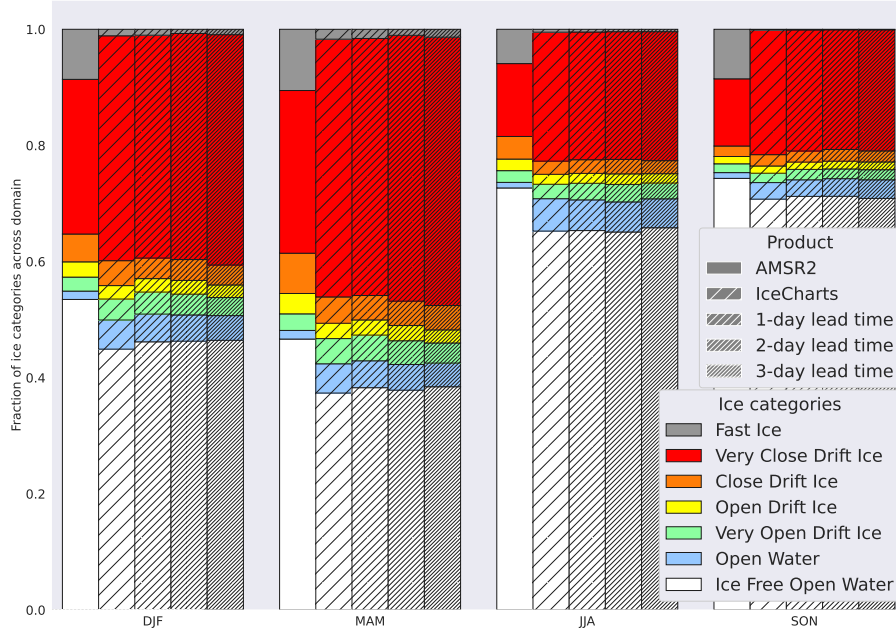


**Figure 5.** Seasonal distribution of each SIC category for 2022 as respective fraction of the total mean SIC area for AMSR2, ice charts and the deep learning system at 1 – 3 day lead time. The AMSR2 data have been projected onto the deep learning model domain.

achieves the lowest nIIEE. Similar to persistence, nIIEE for the deep learning forecasts increases proportionally with lead time, although at a lower rate. Additionally, neither neXtSIM, free-drift nor the linear trend forecast are able to outperform persistence, on average for the 10% concentration contour scoring a factor of 1.57, 1.12, and 1.34 higher than persistence, respectively. Furthermore, the mean nIIEE between forecasts based on ice charts (Deep learning, Persistence and free-drift) and NeXtSIM and the linear trend whom are forced by a different sea ice concentration source is notably shifted from the 70% concentration thresholds and above. However we also trained deep learning models on input AMSR2 passive microwave observations with ice charts as target, and deep learning predictions retained sufficient skill comparable to ice chart persistence yet achieving somewhat higher nIIEE than deep learning models trained on input ice charts (see the Supplement).

The deep learning forecasts improve upon persistence by reducing the  $nIIEE_{10\%}$  by a factor of 0.82. In terms of error-growth as a function of lead-time, the linear trend forecast is the only forecast where the slope of the error increases with increasing lead-time regardless of concentration threshold. This indicates that the linear trend from past OSI SAF SSMIS observations is unable to capture ice chart evolution especially for longer lead times. Moreover, though neXtSIM forecasts have an comparatively high nIIEE initially, the error-growth with lead-time is the lowest for all concentrations, indicating that neXtSIM may provide more useful forecasts at longer lead-times especially for lower concentrations.

Fig. 7 shows how the deep learning system resolves the seasonal variation of the sea ice edge length for different lead times. The predicted sea ice edge follows a similar seasonal pattern to the ice edge length from the target ice charts. Each monthly mean predicted sea ice edge length has a negative bias compared to the ice charts, which increases for longer lead times. Given

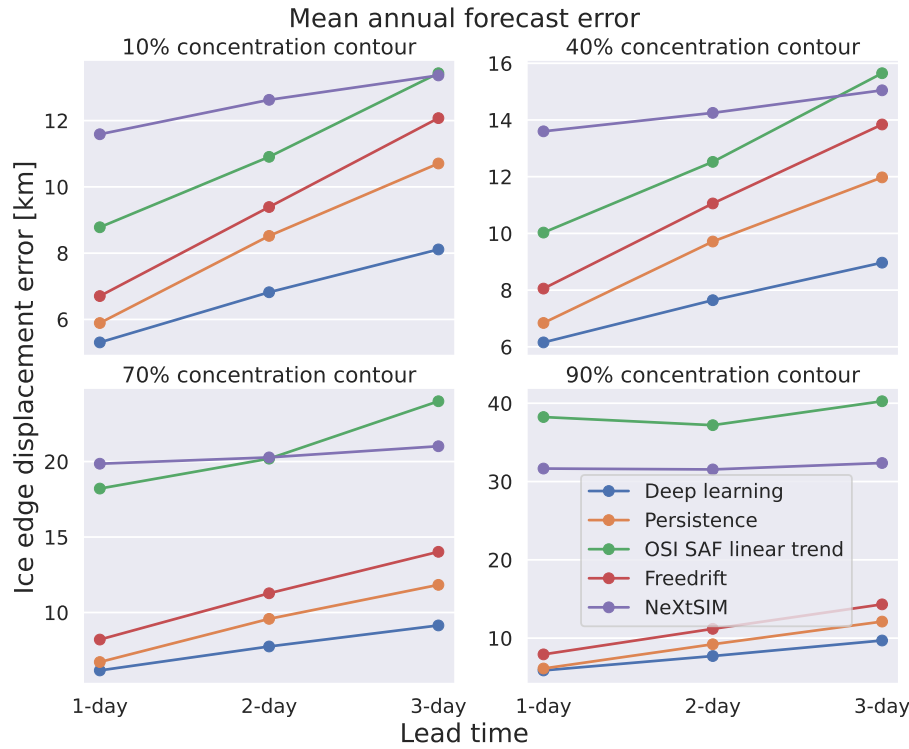


**Figure 6.** Mean annual ice edge displacement error as function of lead time for different sea ice concentration contours defined by 10, 40, 70 and 90% SIC. Only products with a complete coverage of 2022 have been considered. Ice charts are used as reference product.

that the deep learning forecasts resolve the different categories akin to the ice charts, we attribute the apparent negative bias of the length to the lack of details along the forecast contour edges. Hence SIC contour smoothness is somewhat proportional to forecast lead time.

In order to assess the consistency of the deep learning forecasts trained on ice charts, we evaluate the performance by replacing the ice charts with AMSR2 observations as reference dataset in Fig. 8. When utilizing AMSR2 observations as reference, the number of samples used to evaluate the forecasts is consistently 247 across all lead times. We see in Fig. 8 that the deep learning forecasts on average achieves the highest nIIEE when considering a 10% concentration contour, achieving a mean nIIEE<sub>10%</sub> of 16.7 km across the lead times. The displacement is consistent with the inherent nIIEE difference between the AMSR2 observations and the ice charts (Fig. 5), which we found to be 13.3 km for the 10% concentration contour when compared across the test dataset. Furthermore, AMSR2 persistence forecasts achieves the lowest nIIEE on average for the same contour. When considering SIC contours defined by  $\geq 40\%$  SIC, the deep learning forecasts perform closer to AMSR2 persistence, albeit achieving a slightly higher nIIEE on average. neXtSIM on average outperforms the deep learning forecasts for the 10% concentration contour, however this is not the case for the 40, 70 or 90% concentration contours where the performance is close to the initial error for all lead times similar the behaviour in Fig. 6. For the contours higher than 10%



**Figure 7.** Mean monthly sea ice edge length for 2022, with the sea ice edge defined by a 10% concentration threshold. The considered products are the ice charts and deep learning system for 1 – 3 day lead times.

SIC, Fig. 8 shows that AMSR2 persistence, AMSR2 free-drift and the deep learning forecasts on average gradually improve against both neXtSIM and the linear trend, with the deep learning forecast increasing its improvement against neXtSIM for higher contours. The difference between AMSR2 free-drift and AMSR2 persistence can also be seen decreasing for increasing concentration contours, yet AMSR2 free-drift achieves a higher nIIEE than the AMSR2 linear trend considering the 10 and 40% concentration contours. Overall, AMSR2 persistence mostly achieves the lowest nIIEE, although surpassed by the deep learning forecasts when higher concentration contours  $\geq 90\%$  and  $\geq 2$ -day lead time are considered. Moreover, the deep learning forecasts achieve the lowest nIIEE scores when predicting the 40% concentration contour from the AMSR2 observations, in good agreement with the average nIIEE difference between AMSR2 and the ice charts which we found to be 9.7 km for the same concentration contour.

The model intercomparison experiment which compares the deep learning system against baseline- and dynamical sea ice forecasts for all seasons is presented in Fig. 9 using the ice charts as reference. For all considered lead-times and target contours,



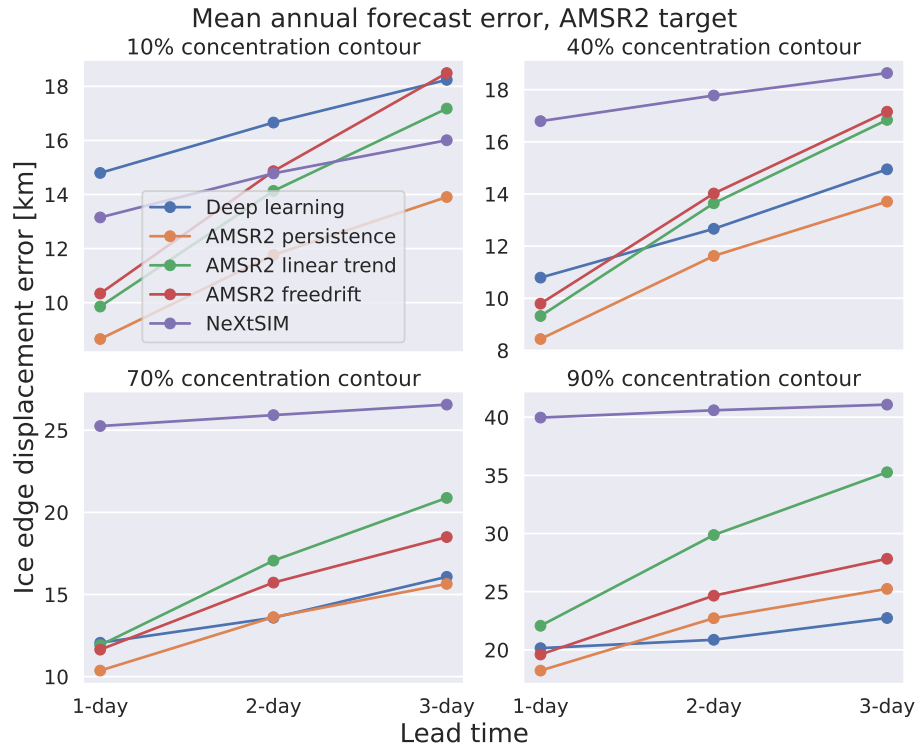


**Figure 8.** Mean annual ice edge displacement error as a function of lead time. The ice edge displacement error for the different products has been computed considering AMSR2 observations as reference.

the deep learning forecasts achieve the lowest seasonal mean nIIEE. The seasonal axis of Fig. 9 shows that both ice chart persistence, free-drift and the deep learning forecasts achieve higher nIIEE values during winter and spring, associating the errors to the periods of freeze-up and sea ice maximum extent. When the nIIEE is computed from the 70 or 90% concentration contours, Fig. 9 shows that the forecasts not utilizing ice chart information (i.e. linear trend, neXtSIM and Barents-2.5) attain considerably higher values, especially during summer. This pattern might indicate a discrepancy between the ice charts, the dynamical forecasts and linear trend with regards to how higher SIC is resolved, further influenced by seasonal conditions.

### 4.3 Feature importance

To better understand the importance of the different predictors used, as well as the sensitivity of the deep learning system to the predictors, we measured how the model responds to modified predictors. In order to measure the impact of each predictor, we first conducted an experiment where the nIIEE was computed from deep learning models fitted to different predictor subsets. The effect of including different predictors on deep learning forecast performance is shown in Fig. 10. In general, removing predictors tends to decrease the predictive skill of the deep learning system, except for 2 meter temperature for 2-day lead time and the past trend for 3-day lead time. Removing the current ice chart has the highest impact on performance (mean

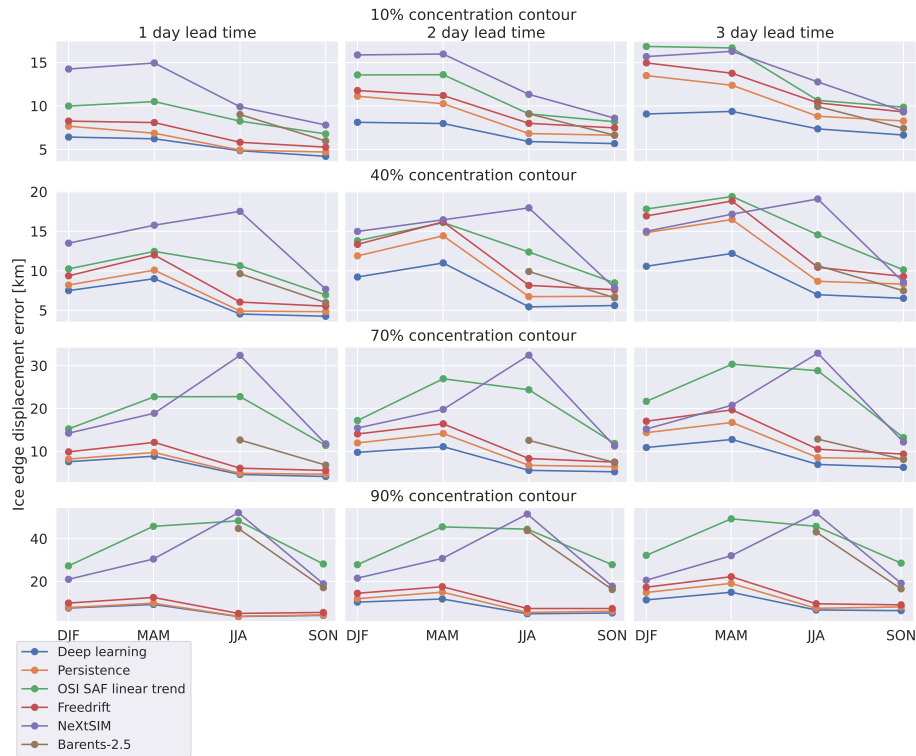


**Figure 9.** Model intercomparison for varying seasons, lead times and concentration contours. The ice charts are considered as reference. The values reported represent the integrated ice edge error normalized according to the length of the current SIC contour from the reference ice chart in km. The OSI SAF linear trend is computed from the past five days. Barents-2.5 results are only shown for summer and fall.

+7.14 km on average for all lead times), reducing the skill of the model below that of persistence. However the impact of removing ice charts is reduced for increasing lead times. Contrarily, the loss of skill associated with removing all AROME Arctic predictors increases with lead time. Although no other combination of held-back predictors decreases the skill of the deep learning forecasts below persistence, removing all atmospheric forecasts has a consistent negative impact to forecast skill (+1.31 km on average) more than any other removed set, except SIC from ice charts. Comparing the impact of the different predictors originating from AROME Arctic shows that removing both wind components simultaneously has a greater effect on forecast skill (+0.86 km) on average than removing 2-meter temperature (+0.08 km). Models trained without the past sea ice trend perform comparably to default deep learning models (+0.06 km).

We also conducted a permutation feature importance analysis to quantify the importance of each predictor for a deep learning model trained on all predictors. Permutation feature importance involves randomly shuffling the input sequence of a single predictor, and analysing how much this alters the predictive skill of the model. To minimize the potential impact of a seasonal cycle appearing in the reordered predictors, the experiment was run 10 times for each predictor. Permutation feature importance is model specific, and does not provide insight into the predictive capabilities of the analysed predictors. Fig. 11 shows the

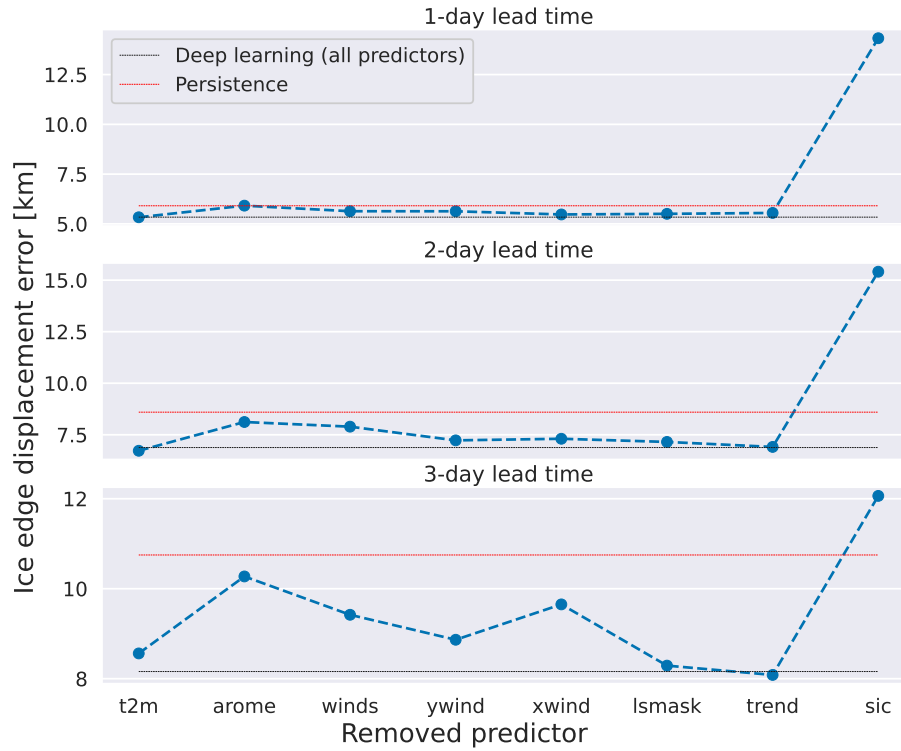


**Figure 10.** Yearly mean nIIEE when a subset of the predictors is withheld during training. The black dashed line denotes yearly mean nIIEE for deep learning forecasts from a model with all predictors, and the red dashed line denotes the skill of persistence. Arome refers to the removal of all atmospheric predictors during training. Winds is similar but for the two wind components.

385 predictor importance evolution over increasing lead times as the difference in ice edge displacement error from the reference  
 deep learning forecasts. Although the importance of each predictor varies with lead time, the order of importance is consistent  
 between all lead times with the recent ice chart being the most important predictor, near surface temperature ranking second  
 and finally the two wind components ranking about equal as the third most important predictors. Only permuted ice charts and  
 near surface temperature significantly decrease deep learning forecast score below the benchmark skill of persistence. Only ice  
 390 charts and 2 meter temperature at 3-day lead time attained a noticeable standard deviation ( $\geq 0.1$  km) from inputting predictors  
 from different dates. There is an inverse proportional relationship between the importance of the recent ice chart (decreasing)  
 and the importance of the atmospheric forecasts (increasing) when targeting longer lead times, indicating that the model is  
 more reliant on the future state of the predicted system (atmospheric forecasts) rather than the initial state (recent ice chart)  
 for longer lead times. Hence Fig. 11 suggests the existence of a limit to the predictive capability gained from providing only  
 395 current sea ice conditions, similar to how persistence and linear trend forecasts inherently lose skill at longer lead times. The  
 skill difference from past sea ice information encoded in the OSI SAF linear trend is indistinguishable (+0.01 km) from the

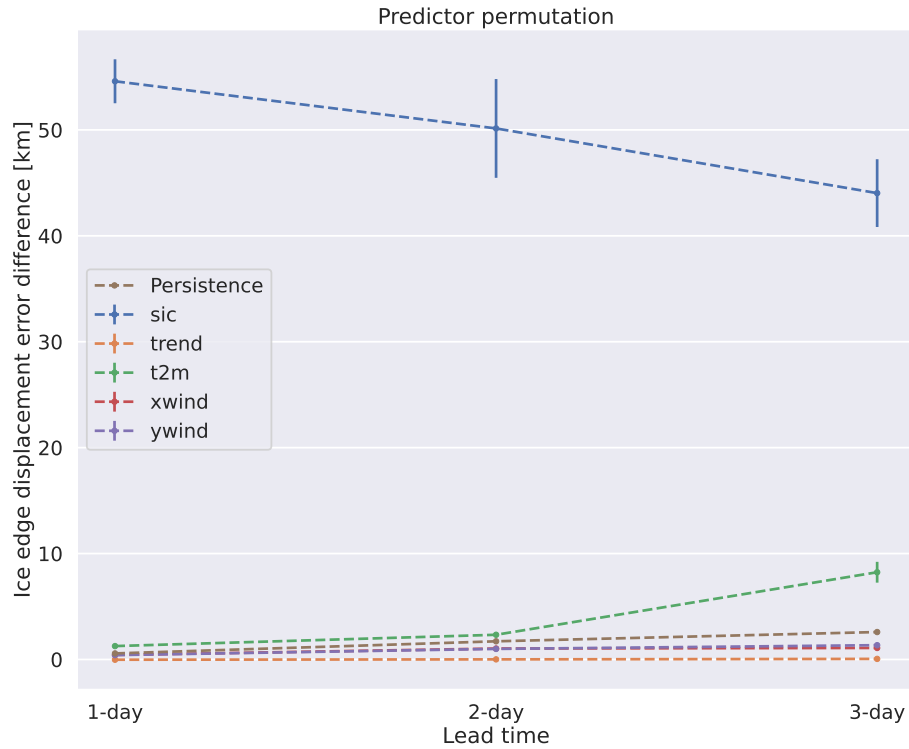


**Figure 11.** Yearly mean nIIEE where the sequence of a predictor in the test dataset has been shuffled, repeated 10 times for all predictors. Each line represents a permuted predictor sequence. Unaltered Persistence forecasts are included as benchmark references. The land-sea mask predictor was excluded from the analysis, as it is static regardless of forecast start-date.

performance of un-permuted deep learning forecasts, hence the deep learning forecasts are not dependent on the past state of sea ice regardless of target lead time.

## 5 Discussion and conclusions

400 This study presents the development of a deep learning forecasting system targeting high resolution (1km) and short lead times (1 – 3 days) taking into account operational constraints related to the real time availability of data. In order to adequately resolve the skewed distribution of SIC classes in the ice charts (especially in the MIZ which is crucial for skillful forecasts ensuring maritime safety (Wagner et al., 2020)), we present a novel reformulation of the target data and decoder from the original U-Net architecture of Ronneberger et al. (2015) which we name cumulative contours (Eq. 1). The cumulative contours demonstrate  
405 how combining architectural design from Multi-Task learning (Zhang et al., 2014) with task specific additive properties of SIC intervals positively benefit to deep learning forecasting skill, especially for resolving the intermediate SIC intervals constituting the MIZ. With this reformulation of the U-Net, the deep learning forecasts are able to consistently outperform the baseline

forecasts as well as operational short-range dynamical sea ice forecasting systems (neXtSIM-F and Barents-2.5) in terms of achieving the lowest ice edge displacement error when considering the ice charts as reference.

410 Despite training deep learning models to predict SIC conditions from the ice charts only, the deep learning forecasts behave similarly to baseline-forecasts when validated against independent AMSR2 SIC observations (Spren et al., 2008) for concentration contours  $\geq 40\%$ . The increase in deep learning performance seen between the 10% and 40% concentration contours may be indicative of a shift in SIC distribution for lower concentration values between the two products, as further indicated by the increased similarity in occurrence frequency between AMSR2 and the ice charts when considering open and close drift  
415 ice reported in Fig. 5. It is noted that the ASI sea ice retrieval algorithm exerts larger uncertainties for lower concentrations (Spren et al., 2008), whereas  $SIC < 10\%$  is visible in SAR and optical satellite images used by the ice analysts drawing ice charts. However ice charts are influenced by human decision-making especially in the medium concentrations (40 – 70%) of the MIZ (Dinessen et al., 2020), which may be sources for ice edge location discrepancy between the two products. The overall performance regardless of reference product suggests a degree of consistency for the developed forecasts between the two  
420 reference products. However the analysis also suggests that inherent differences between sea ice products is reflected by deep learning forecasts, and we can not expect the forecasts to improve beyond that initial difference as the models are trained to only minimize the statistical error of their target sea ice product.

The results from the forecast intercomparison analysis demonstrates that the deep learning forecasts meet the requirements for forecast accuracy, while considerably reducing the computing time. However, the results from the analysis could be influ-  
425 enced by the uneven sample sizes used for verification at different lead times. Hence we recommend evaluating the forecasts with longer time series when they become available. With respect to the development of the operational weather prediction system AROME Arctic, a continued forecast evaluation can also facilitate understanding model response to continuously updated atmospheric predictors and the potential of fine-tuning deep learning models. With regards to operationalization, the input data supplied to the deep learning forecasting system have been chosen with considerations of publishing time, with a special  
430 constraint for AROME Arctic being the 66 hour forecast length. The current setup allows three day forecasts to be published every weekday, sent to maritime operators in advance of their valid date and cover Saturdays and Sundays when Norwegian ice charts are not produced.

The predictor importance analysis suggests that the deep learning models benefit from an increased and diversified dataset by increasing the precision of the predicted sea ice edge by 1.31 km when atmospheric forecasts from AROME Arctic (Müller  
435 et al., 2017) are included as predictors. The inclusion of forecast predictors from weather forecasts has previously been shown to increase predictive skill (Grigoryev et al., 2022; Palerme et al., 2024), which further motivates the inclusion of other forecasted physical forcings affecting the sea ice as predictors. We recommend further work to investigate currently unexplored metocean forcings such as ice-wave interactions (Williams et al., 2013) by including fields such as forecasted wave height and wave direction. However, expanding the dataset towards past temporal regimes by including a coarse resolution linear SIC trend  
440 derived from OSI SAF observations was shown to have a marginal effect on the forecast skill, indicating that the deep learning models were unable to infer sea ice growth / decline from past observations (Fig. 11), in line with the results of Palerme et al. (2024).

When all predictors were provided as inputs to the deep learning models, the skill of the forecasts was particularly sensitive to the initialization date of the inputted ice chart (Fig. 11). This suggests that a large part of the inferred physics and seasonality originates from the ice charts, which can also explain why the atmospheric predictors were not essential to outperform persistence. Additionally the comparison made against free-drift SIC forecasts suggests that the deep learning model has learned a relationship between the input predictors and target ice chart which is beyond a sea ice motion estimation linearly proportional to the near surface winds. Although it is unknown how the deep learning model respond to individual predictors, the comparison suggests that the models' ability to learn non-linear relationships in the input data helps in predicting SIC. Moreover, the comparison suggests that inferring thermodynamical properties that allow the model to grow and melt sea ice aids when predicting short term SIC beyond that of advection.

When considering the initialization time of the AROME Arctic predictors, the lessened impact of the atmospheric predictors could also be associated with AROME Arctic not covering the beginning of the forecast period, especially for shorter lead times. Nevertheless as the model sensitivity to the current ice chart tends to decrease for longer lead times, understanding how the model utilizes the increasingly important forecast predictors should be considered, especially when targeting longer lead times. Other works have investigated the use of explainable artificial intelligence methodologies for interpreting climate-science deep neural networks models and results (e.g. Toms et al., 2020; Ebert-Uphoff and Hilburn, 2020; Bommer et al., 2023). This should be given more attention as they present an opportunity to develop new tools for diagnosing machine learning sea ice forecasting systems.

*Code and data availability.* All code necessary to deploy the developed deep learning models, as well as pretrained weights, are available on the following GitHub repository: [https://github.com/AreFrode/Developing\\_ice\\_chart\\_deep\\_learning\\_predictions](https://github.com/AreFrode/Developing_ice_chart_deep_learning_predictions). AROME Arctic (<https://thredds.met.no/thredds/catalog/aromearcticarchive/catalog.html>) and Barents-2.5 ([https://thredds.met.no/thredds/catalog/barents25km\\_files/catalog.html](https://thredds.met.no/thredds/catalog/barents25km_files/catalog.html)) forecasts, as well as OSI SAF SSMIS sea ice concentration observations (<https://thredds.met.no/thredds/catalog/osisaf/met.no/ice/conc/catalog.html>) can be downloaded from the MET Norway thredds Data Server (missing Barents-2.5 data can be provided upon request). The ASI AMSR2 sea ice concentration observations are available on the University of Bremen Sea Ice Remote Sensing data archive ([https://data.seaice.uni-bremen.de/amr2/asi\\_daygrid\\_swath/n6250/](https://data.seaice.uni-bremen.de/amr2/asi_daygrid_swath/n6250/)). Gridded Norwegian Ice Service ice charts and neXtSIM data can be provided upon request.

## Appendix A: Comparing nIIEE for high- and low resolution sea ice concentration

In order to evaluate 1 km resolution sea ice forecasts using the ice edge displacement error as derived by Melsom et al. (2019), we assess the validity of applying the metric for high resolution sea ice forecasts by comparing against a coarse resolution (10 km) reference case. We compute nIIEE from the ice charts at 2-day lead time persistence, with ice charts at 1 km resolution as well as downsampled onto a 10 km grid covering the period 2019 – 2020. Mean monthly nIIEE for both forecasts are shown in Fig. A1. The correlation coefficient between both nIIEE curves in Fig. A1 is 0.98. The strong correlation indicates that the nIIEE is preserved when used in a 1 km resolution environment.

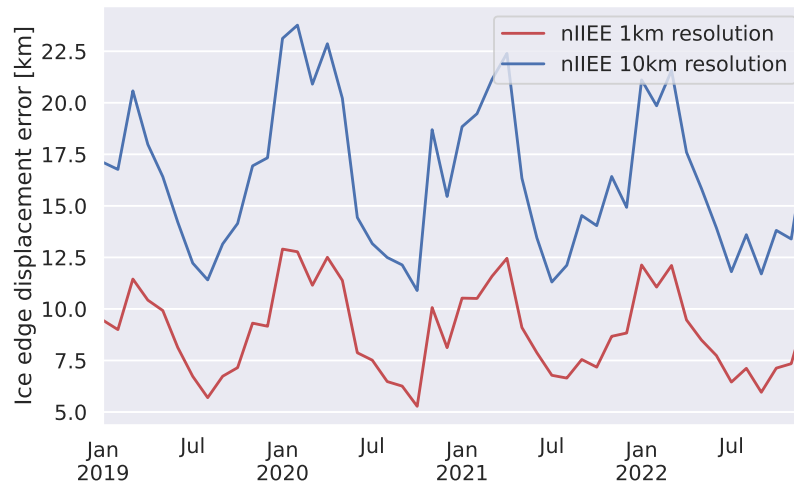


**Figure A1.** nIIEE computed across the entirety of the training dataset (2019 – 2022) for 2-day lead time ice chart persistence with the ice charts as reference. The sea ice edge length used to divide the compute IIEE was derived from the same resolution as the respective forecast.

475 *Author contributions.* A.F.K. conceptualization, analysis, methodology, original draft preparation. C.P. conceptualization, analysis, methodology, review & editing, supervision. M.M. conceptualization, analysis, review & editing, supervision. J.R. conceptualization, analysis, review & editing. N.H. gridded ice charts, review & editing.

*Competing interests.* The authors declare that they have no conflict of interest

480 *Acknowledgements.* This work has been supported by the DigitalSeaIce – Multi-scale integration and digitalization of Arctic sea ice observations and prediction models project, which is funded by the Research Council of Norway under contract 328960. C.P. acknowledges support from the SEAFARING project supported by the Norwegian Space Agency and the Copernicus Marine Service COSI project. Copernicus Marine Service is implemented by Mercator Ocean in the framework of a delegation agreement with the European Union. J.R. gratefully acknowledges the support by the Research Council of Norway through the MachineOcean project (grant No. 303411). The authors would like to thank Julien Brajard for constructive discussions.

- Andersson, T. R., Hosking, J. S., Pérez-Ortiz, M., Paige, B., Elliott, A., Russell, C., Law, S., Jones, D. C., Wilkinson, J., Phillips, T., Byrne, J., Tietsche, S., Sarojini, B. B., Blanchard-Wrigglesworth, E., Aksenov, Y., Downie, R., and Shuckburgh, E.: Seasonal Arctic sea ice forecasting with probabilistic deep learning, *Nature Communications*, 12, <https://doi.org/10.1038/s41467-021-25257-4>, 2021.
- 490 Batrak, Y. and Müller, M.: On the warm bias in atmospheric reanalyses induced by the missing snow over Arctic sea-ice, *Nature Communications*, 10, <https://doi.org/10.1038/s41467-019-11975-3>, 2019.
- Blair, B., Müller, M., Palerme, C., Blair, R., Crookall, D., Knol-Kauffman, M., and Lamers, M.: Coproducing Sea Ice Predictions with Stakeholders Using Simulation, *Weather, Climate, and Society*, 14, 399–413, <https://doi.org/10.1175/wcas-d-21-0048.1>, 2022.
- Bommer, P., Kretschmer, M., Hedström, A., Bareeva, D., and Höhne, M. M. C.: Finding the right XAI method – A Guide for the Evaluation and Ranking of Explainable AI Methods in Climate Science, <https://doi.org/10.48550/ARXIV.2303.00652>, 2023.
- 495 Cavalieri, D., Parkinson, C., Gloersen, P., and Zwally, H. J.: Sea Ice Concentrations from Nimbus-7 SMMR and DMSP SSM/I-SSMIS Passive Microwave Data, Version 1, <https://doi.org/10.5067/8GQ8LZQVL0VL>, 1996.
- Comiso, J. C., Meier, W. N., and Gersten, R.: Variability and trends in the Arctic Sea ice cover: Results from different techniques, *Journal of Geophysical Research: Oceans*, 122, 6883–6900, <https://doi.org/10.1002/2017jc012768>, 2017.
- Dinessen, F., Hackett, B., and Kreiner, M. B.: Product User Manual For Regional High Resolution Sea Ice Charts Svalbard and Greenland Region, Tech. rep., Norwegian Meteorological Institute, 2020.
- 500 Ebert-Uphoff, I. and Hilburn, K.: Evaluation, Tuning, and Interpretation of Neural Networks for Working with Images in Meteorological Applications, *Bulletin of the American Meteorological Society*, 101, E2149–E2170, <https://doi.org/10.1175/bams-d-20-0097.1>, 2020.
- Eguíluz, V. M., Fernández-Gracia, J., Irigoien, X., and Duarte, C. M.: A quantitative assessment of Arctic shipping in 2010–2014, *Scientific Reports*, 6, <https://doi.org/10.1038/srep30682>, 2016.
- 505 Fritzner, S., Graverson, R., and Christensen, K. H.: Assessment of High-Resolution Dynamical and Machine Learning Models for Prediction of Sea Ice Concentration in a Regional Application, *Journal of Geophysical Research: Oceans*, 125, <https://doi.org/10.1029/2020jc016277>, 2020.
- Goessling, H. F., Tietsche, S., Day, J. J., Hawkins, E., and Jung, T.: Predictability of the Arctic sea ice edge, *Geophysical Research Letters*, 43, 1642–1650, <https://doi.org/10.1002/2015gl067232>, 2016.
- 510 Grigoryev, T., Verezemskaya, P., Krinitskiy, M., Anikin, N., Gavrikov, A., Trofimov, I., Balabin, N., Shpilman, A., Eremchenko, A., Gulev, S., Burnaev, E., and Vanovskiy, V.: Data-Driven Short-Term Daily Operational Sea Ice Regional Forecasting, *Remote Sensing*, 14, <https://doi.org/10.3390/rs14225837>, 2022.
- Gunnarsson, B.: Recent ship traffic and developing shipping trends on the Northern Sea Route—Policy implications for future arctic shipping, *Marine Policy*, 124, 104 369, <https://doi.org/10.1016/j.marpol.2020.104369>, 2021.
- 515 He, K., Zhang, X., Ren, S., and Sun, J.: Delving Deep into Rectifiers: Surpassing Human-Level Performance on ImageNet Classification, <https://doi.org/10.48550/ARXIV.1502.01852>, 2015.
- Hersbach, H., Bell, B., Berrisford, P., Hirahara, S., Horányi, A., Muñoz-Sabater, J., Nicolas, J., Peubey, C., Radu, R., Schepers, D., Simmons, A., Soci, C., Abdalla, S., Abellan, X., Balsamo, G., Bechtold, P., Biavati, G., Bidlot, J., Bonavita, M., De Chiara, G., Dahlgren, P., Dee, D., Diamantakis, M., Dragani, R., Flemming, J., Forbes, R., Fuentes, M., Geer, A., Haimberger, L., Healy, S., Hogan, R. J.,
- 520 Hólm, E., Janisková, M., Keeley, S., Laloyaux, P., Lopez, P., Lupu, C., Radnoti, G., de Rosnay, P., Rozum, I., Vamborg, F., Vil-



- laume, S., and Thépaut, J.-N.: The ERA5 global reanalysis, *Quarterly Journal of the Royal Meteorological Society*, 146, 1999–2049, <https://doi.org/https://doi.org/10.1002/qj.3803>, 2020.
- Hunke, E. C., Lipscomb, W. H., Turner, A. K., Jeffery, N., and Elliott, S.: CICE: the Los Alamos Sea Ice Model Documentation and Software User’s Manual Version 5.1 LA-CC-06-012, techreport, Los Alamos National Laboratory, Los Alamos NM 87545, 2015.
- 525 Johnson, S. J., Stockdale, T. N., Ferranti, L., Balmaseda, M. A., Molteni, F., Magnusson, L., Tietsche, S., Decremmer, D., Weisheimer, A., Balsamo, G., Keeley, S. P. E., Mogensen, K., Zuo, H., and Monge-Sanz, B. M.: SEAS5: the new ECMWF seasonal forecast system, *Geoscientific Model Development*, 12, 1087–1117, <https://doi.org/10.5194/gmd-12-1087-2019>, 2019.
- Kingma, D. P. and Ba, J.: Adam: A Method for Stochastic Optimization, <https://doi.org/10.48550/ARXIV.1412.6980>, 2014.
- Kucik, A. and Stokholm, A.: AI4SeaIce: selecting loss functions for automated SAR sea ice concentration charting, *Scientific Reports*, 13, 530 <https://doi.org/10.1038/s41598-023-32467-x>, 2023.
- Kwok, R.: Arctic sea ice thickness, volume, and multiyear ice coverage: losses and coupled variability (1958–2018), *Environmental Research Letters*, 13, 105 005, <https://doi.org/10.1088/1748-9326/aae3ec>, 2018.
- Lavergne, T., Sørensen, A. M., Kern, S., Tonboe, R., Notz, D., Aaboe, S., Bell, L., Dybkjær, G., Eastwood, S., Gabarro, C., Heygster, G., Killie, M. A., Brandt Kreiner, M., Lavelle, J., Saldo, R., Sandven, S., and Pedersen, L. T.: Version 2 of the EUMETSAT OSI SAF and 535 ESA CCI sea-ice concentration climate data records, *The Cryosphere*, 13, 49–78, <https://doi.org/10.5194/tc-13-49-2019>, 2019.
- Liu, Q., Zhang, R., Wang, Y., Yan, H., and Hong, M.: Short-Term Daily Prediction of Sea Ice Concentration Based on Deep Learning of Gradient Loss Function, *Frontiers in Marine Science*, 8, <https://doi.org/10.3389/fmars.2021.736429>, 2021a.
- Liu, Y., Bogaardt, L., Attema, J., and Hazeleger, W.: Extended Range Arctic Sea Ice Forecast with Convolutional Long-Short Term Memory Networks, *Monthly Weather Review*, <https://doi.org/10.1175/mwr-d-20-0113.1>, 2021b.
- 540 Long, J., Shelhamer, E., and Darrell, T.: Fully convolutional networks for semantic segmentation, in: 2015 IEEE Conference on Computer Vision and Pattern Recognition (CVPR), IEEE, <https://doi.org/10.1109/cvpr.2015.7298965>, 2015.
- Melsom, A., Palerme, C., and Müller, M.: Validation metrics for ice edge position forecasts, *Ocean Science*, 15, 615–630, <https://doi.org/10.5194/os-15-615-2019>, 2019.
- Metzger, E. J., Smedstad, O. M., Thoppil, P., Hurlburt, H., Cummings, J., Walcraft, A., Zamudio, L., Franklin, D., Posey, P., Phelps, M., 545 Hogan, P., Bub, F., and DeHaan, C.: US Navy Operational Global Ocean and Arctic Ice Prediction Systems, *Oceanography*, 27, 32–43, <https://doi.org/10.5670/oceanog.2014.66>, 2014.
- Müller, M., Batrak, Y., Kristiansen, J., Køltzow, M. A. Ø., Noer, G., and Korosov, A.: Characteristics of a Convective-Scale Weather Forecasting System for the European Arctic, *Monthly Weather Review*, 145, 4771–4787, <https://doi.org/10.1175/mwr-d-17-0194.1>, 2017.
- Müller, M., Knol-Kauffman, M., Jeuring, J., and Palerme, C.: Arctic shipping trends during hazardous weather and sea-ice conditions and 550 the Polar Code’s effectiveness, *npj Ocean Sustainability*, 2, <https://doi.org/10.1038/s44183-023-00021-x>, 2023.
- Nair, V. and Hinton, G.: Rectified Linear Units Improve Restricted Boltzmann Machines Vinod Nair, in: ICML’10: Proceedings of the 27th International Conference on International Conference on Machine Learning, vol. 27, pp. 807–814, 2010.
- Notz, D. and Community, S.: Arctic Sea Ice in CMIP6, *Geophysical Research Letters*, 47, <https://doi.org/10.1029/2019gl086749>, 2020.
- Notz, D. and Marotzke, J.: Observations reveal external driver for Arctic sea-ice retreat, *Geophysical Research Letters*, 39, 555 <https://doi.org/10.1029/2012gl051094>, 2012.
- Ólason, E., Boutin, G., Korosov, A., Rampal, P., Williams, T., Kimmritz, M., Dansereau, V., and Samaké, A.: A New Brittle Rheology and Numerical Framework for Large-Scale Sea-Ice Models, *Journal of Advances in Modeling Earth Systems*, 14, <https://doi.org/10.1029/2021ms002685>, 2022.

- Owens, R. and Hewson, T.: ECMWF Forecast User Guide, <https://doi.org/10.21957/M1CS7H>, 2018.
- 560 Palerme, C., Müller, M., and Melsom, A.: An Intercomparison of Verification Scores for Evaluating the Sea Ice Edge Position in Seasonal Forecasts, *Geophysical Research Letters*, 46, 4757–4763, <https://doi.org/10.1029/2019gl082482>, 2019.
- Palerme, C., Lavergne, T., Rusin, J., Melsom, A., Brajard, J., Kvanum, A. F., Macdonald Sørensen, A., Bertino, L., and Müller, M.: Improving short-term sea ice concentration forecasts using deep learning, *The Cryosphere*, 18, 2161–2176, <https://doi.org/10.5194/tc-18-2161-2024>, 2024.
- 565 Rainville, L., Wilkinson, J., Durley, M. E. J., Harper, S., DiLeo, J., Doble, M. J., Fleming, A., Forcucci, D., Graber, H., Hargrove, J. T., Haverlack, J., Hughes, N., Hembrough, B., Jeffries, M. O., Lee, C. M., Mendenhall, B., McCormick, D., Montalvo, S., Stenseth, A., Shilling, G. B., Simmons, H. L., Toomey, J. E., and Woods, J.: Improving Situational Awareness in the Arctic Ocean, *Frontiers in Marine Science*, 7, <https://doi.org/10.3389/fmars.2020.581139>, 2020.
- Rampal, P., Bouillon, S., Ólason, E., and Morlighem, M.: neXtSIM: a new Lagrangian sea ice model, *The Cryosphere*, 10, 1055–1073, <https://doi.org/10.5194/tc-10-1055-2016>, 2016.
- 570 Ren, Y., Li, X., and Zhang, W.: A Data-Driven Deep Learning Model for Weekly Sea Ice Concentration Prediction of the Pan-Arctic During the Melting Season, *IEEE Transactions on Geoscience and Remote Sensing*, 60, 1–19, <https://doi.org/10.1109/tgrs.2022.3177600>, 2022.
- Ronneberger, O., Fischer, P., and Brox, T.: U-Net: Convolutional Networks for Biomedical Image Segmentation, in: *Lecture Notes in Computer Science*, pp. 234–241, Springer International Publishing, [https://doi.org/10.1007/978-3-319-24574-4\\_28](https://doi.org/10.1007/978-3-319-24574-4_28), 2015.
- 575 Röhrs, J., Gusdal, Y., Rikardsen, E. S. U., Moro, M. D., Brændshøj, J., Kristensen, N. M., Fritzner, S., Wang, K., Sperrevik, A. K., Idžanović, M., Lavergne, T., Debernard, J. B., and Christensen, K. H.: Barents-2.5km v2.0: an operational data-assimilative coupled ocean and sea ice ensemble prediction model for the Barents Sea and Svalbard, *Geoscientific Model Development*, 16, 5401–5426, <https://doi.org/10.5194/gmd-16-5401-2023>, 2023.
- Sakov, P., Counillon, F., Bertino, L., Lisæter, K. A., Oke, P. R., and Korabiev, A.: TOPAZ4: an ocean-sea ice data assimilation system for the North Atlantic and Arctic, *Ocean Science*, 8, 633–656, <https://doi.org/10.5194/os-8-633-2012>, 2012.
- 580 Serreze, M. C. and Barry, R. G.: Processes and impacts of Arctic amplification: A research synthesis, *Global and Planetary Change*, 77, 85–96, <https://doi.org/10.1016/j.gloplacha.2011.03.004>, 2011.
- Serreze, M. C. and Meier, W. N.: The Arctic’s sea ice cover: trends, variability, predictability, and comparisons to the Antarctic, *Annals of the New York Academy of Sciences*, 1436, 36–53, <https://doi.org/https://doi.org/10.1111/nyas.13856>, 2019.
- 585 Spreen, G., Kaleschke, L., and Heygster, G.: Sea ice remote sensing using AMSR-E 89-GHz channels, *Journal of Geophysical Research*, 113, <https://doi.org/10.1029/2005jc003384>, 2008.
- Stocker, A. N., Renner, A. H. H., and Knol-Kauffman, M.: Sea ice variability and maritime activity around Svalbard in the period 2012–2019, *Scientific Reports*, 10, <https://doi.org/10.1038/s41598-020-74064-2>, 2020.
- Toms, B. A., Barnes, E. A., and Ebert-Uphoff, I.: Physically Interpretable Neural Networks for the Geosciences: Applications to Earth System Variability, *Journal of Advances in Modeling Earth Systems*, 12, <https://doi.org/10.1029/2019ms002002>, 2020.
- 590 Veland, S., Wagner, P., Bailey, D., Everett, A., Goldstein, M., Hermann, R., Hjort-Larsen, T., Hovelsrud, G., Hughes, N., Kjøl, A., Li, X., Lynch, A., Müller, M., Olsen, J., Palerme, C., Pedersen, J. L., Rinaldo, Ø., Stephenson, S., and Storelvmo, T.: Knowledge needs in sea ice forecasting for navigation in Svalbard and the High Arctic, Tech. Rep. NF-rapport 4/2021, Svalbard Strategic Grant, Svalbard Science Forum, 2021.

- 595 Wagner, P. M., Hughes, N., Bourbonnais, P., Stroeve, J., Rabenstein, L., Bhatt, U., Little, J., Wiggins, H., and Fleming, A.: Sea-ice information and forecast needs for industry maritime stakeholders, *Polar Geography*, 43, 160–187, <https://doi.org/10.1080/1088937x.2020.1766592>, 2020.
- Wang, L., Scott, K., and Clausi, D.: Sea Ice Concentration Estimation during Freeze-Up from SAR Imagery Using a Convolutional Neural Network, *Remote Sensing*, 9, 408, <https://doi.org/10.3390/rs9050408>, 2017.
- 600 Williams, T., Korosov, A., Rampal, P., and Ólason, E.: Presentation and evaluation of the Arctic sea ice forecasting system neXtSIM-F, *The Cryosphere*, 15, 3207–3227, <https://doi.org/10.5194/tc-15-3207-2021>, 2021.
- Williams, T. D., Bennetts, L. G., Squire, V. A., Dumont, D., and Bertino, L.: Wave–ice interactions in the marginal ice zone. Part 1: Theoretical foundations, *Ocean Modelling*, 71, 81–91, <https://doi.org/10.1016/j.ocemod.2013.05.010>, 2013.
- Wu, Y. and He, K.: Group Normalization, <https://doi.org/10.48550/ARXIV.1803.08494>, 2018.
- 605 Yu, X., Rinke, A., Dorn, W., Spreen, G., Lüpkes, C., Sumata, H., and Gryanik, V. M.: Evaluation of Arctic sea ice drift and its dependency on near-surface wind and sea ice conditions in the coupled regional climate model HIRHAM–NAOSIM, *The Cryosphere*, 14, 1727–1746, <https://doi.org/10.5194/tc-14-1727-2020>, 2020.
- Zampieri, L., Goessling, H. F., and Jung, T.: Predictability of Antarctic Sea Ice Edge on Subseasonal Time Scales, *Geophysical Research Letters*, 46, 9719–9727, <https://doi.org/10.1029/2019gl084096>, 2019.
- 610 Zhang, L., Shi, Q., Leppäranta, M., Liu, J., and Yang, Q.: Estimating Winter Arctic Sea Ice Motion Based on Random Forest Models, *Remote Sensing*, 16, 581, <https://doi.org/10.3390/rs16030581>, 2024.
- Zhang, Z., Luo, P., Loy, C. C., and Tang, X.: Facial Landmark Detection by Deep Multi-task Learning, in: *Computer Vision – ECCV 2014*, pp. 94–108, Springer International Publishing, [https://doi.org/10.1007/978-3-319-10599-4\\_7](https://doi.org/10.1007/978-3-319-10599-4_7), 2014.